PERGAMON

Electrochimica Acta 44 (1998) 983–992

ELECTROCHIMICA Acta

Electrodeposition dynamics: electrochemical and X-ray scattering studies

E. Herrero [a], L.J. Buller [a,c], J. Li [a], A.C. Finnefrock [b,c], A.B. Salomón [d], C. Alonso [d], J.D. Brock [b,c], H.D. Abruña [a,c,*]

[a] *Department of Chemistry, Cornell University, Ithaca, NY 14853, USA*
[b] *School of Applied and Engineering Physics, Cornell University, Ithaca, NY 14853, USA*
[c] *Materials Science Center, Cornell University, Ithaca, NY 14853, USA*
[d] *Departamento Química Física Aplicada, Univ. Autónoma de Madrid, Madrid, Spain*

Received 11 November 1997; received in revised form 22 December 1997

Abstract

Studies of the electrodeposition dynamics of underpotential deposition (UPD) processes based on electrochemical and in-situ surface X-ray scattering studies are presented. The studies focus on the UPD of Hg on Au(111) in sulfate media, and Cu UPD on Pt(111) in sulfate and chloride media. In the first case it is shown that Hg UPD on Au(111) in sulfuric acid follows a progressive nucleation mechanism which involves various surface structures. In the case of Cu UPD on Pt(111), the process appears to follow an instantaneous nucleation mechanism in both sulfate and chloride media. Time-resolved surface X-ray scattering studies of Cu UPD on Pt(111) in the presence of chloride demonstrate that the electrochemical relaxation and the achievement of long range order can take place on significantly different time scales. Analysis of time-resolved surface X-ray scattering data allows for the study of the dynamics of island growth.

1. Introduction

The underpotential deposition (UPD) of metals onto foreign metal substrates offers the opportunity for studying the early stages of metal deposition [1, 2]. In recent years, the use of single-crystal electrodes in conjunction with in-situ surface techniques, including STM [3–6], AFM [7, 8] and surface X-ray based techniques [8–13], has allowed a detailed investigation of UPD processes. Of particular importance in this regard has been the ability to characterize the different surface structures formed at different potentials and to correlate them with their voltammetric behavior. However, kinetic studies of UPD processes have received considerably less attention [14–21]. Such studies are especially revealing and valuable when detailed potential-dependent structural information is available, since it allows for a direct correlation of the different surface structures with the kinetics of the processes involved. However, the number of studies where kinetic and structural information is available is quite limited. In one such example, Kolb and coworkers [20, 21] investigated the kinetics of copper UPD on Au(111) electrodes and made correlations with structural information. They found that the process followed an instantaneous nucleation mechanism, likely controlled by the density of defect sites on the surface. In addition, it is well established that anions can have significant effects on both the structure and dynamics of formation of UPD monolayers.

In this manuscript, we present a comparative study of the kinetics of mercury UPD on Au(111) electrodes in the presence of bisulfate anions and copper UPD on Pt(111) in the presence of bisulfate and chloride anions. This study focuses on the formation/disruption of the ordered structures formed on the electrode surface. Previous structural studies are employed to arrive

* Corresponding author.

0013-4686/98/$ - see front matter
PII: S0013-4686(98)00202-3

at a more detailed description of the electrodeposition process. In these investigations, we emphasize the importance of data from complementary techniques such as potential step chronoamperometry and grazing incident X-ray diffraction (GIXD).

2. Experimental

Two different sized Au(111) and Pt(111) electrodes were employed in these studies. The larger ones (of ca. 0.9 cm diameter) were grown from the melt at the Materials Science Center at Cornell University and were cut and polished with a miscut of less than 0.3°. The smaller crystals (of ca. 2 mm diameter) were prepared according to Clavilier's technique with a miscut of less than 0.1°. Prior to any measurements, the electrodes were flame-annealed, quenched with ultrapure water [22] and transferred to the cell for electrochemical measurements.

Potential step chronoamperometric measurements were carried out in a U-shaped two-compartment electrochemical cell in the hanging meniscus configuration. Particular care was taken to minimize iR drops so that current transients would not be affected. The transients obtained with both electrodes were the same, in both current density and shape, a clear indication that iR drops are not affecting the measurements. Electrochemical experiments were carried out with a PAR 283 potentiostat interfaced with Corrware® software.

In chronoamperometric current transients, the potential was stepped from an initial potential where a given structure of the adlayer is found to a final potential where partial or total dissolution took place. In a complete series of experiments, the final potential is moved in 2 mV steps.

X-ray diffraction experiments were performed at the X20A beamline at the National Synchrotron Light Source using a four circle diffractometer using an energy of 8.80 keV. The sample cell has a reflection geometry and is similar to those used by others in previous studies [23–25]. X-ray photons penetrate through a 2.5 μm Mylar film (Chemplex) as well as a thin film of electrolyte (estimated to be about 30 μm) covering the crystal. To prevent the diffusion of oxygen from air through the Mylar film, an outer shield with a Kapton window (Chemplex) was placed on top of the sample cell and continuously flushed with ultra pure N_2. Cyclic voltammograms in the X-ray cell were carried out with the Mylar film inflated by adding deoxygenated electrolyte solution. For X-ray measurements, some electrolyte was withdrawn so that the Mylar film was pressed against the crystal surface thus achieving a thin layer configuration. Pt(111) and the Au(111) surfaces are described in terms of a hexagonal lattice with the c axis along the ⟨111⟩ direction and $a = b = 2.774$ Å for platinum and $a = b = 2.885$ Å for gold, respectively.

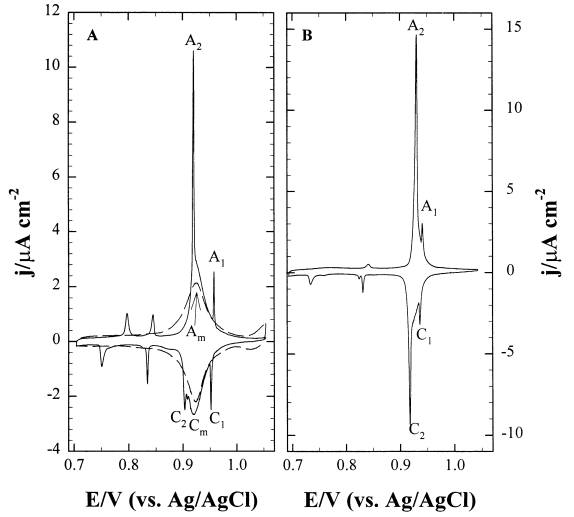

Fig. 1. Voltammetric profile of a Au(111) electrode in (A) 0.10 M $HClO_4$ + 1.0 mM Hg^{2+} (dashed line), 0.10 M $HClO_4$ + 1.0 mM H_2SO_4 + 1.0 mM Hg^{2+} (full line) and (B) 0.10 M H_2SO_4 + 1.0 mM Hg^{2+}. Scan rate: 1 mV s^{-1}.

All potentials were measured and are reported versus a Ag/AgCl electrode in 3 M NaCl. A large area coiled gold (platinum) wire was used as a counterelectrode. All experiments were carried out at room temperature. Solutions were prepared using ultrapure water (18 MOhms Millipore® Milli-Q® water), $HClO_4$ (doubly distilled, 70%, GFS Chemicals), H_2SO_4 (Ultrex J.T. Baker), NaCl (99.999%, Aldrich), CuO (99.999, Aldrich) and HgO (99.998%, Alfa).

3. Results and discussion

3.1. Kinetics of Hg UPD on Au(111) in presence of bisulfate anions

Cyclic voltammograms of mercury UPD between +1.05 and +0.70 V in three different supporting electrolytes at a solution mercury concentration of 1.0 mM are shown in Fig. 1. As can be seen, the presence of (bi)sulfate anions in the solution exerts a significant influence on the voltammetric behavior of mercury UPD on Au(111). In the absence of (bi)sulfate anions (i.e. in 0.1 M $HClO_4$), only one pair of peaks (C_m/A_m) with a Gaussian-like shape appears in the voltammetric profile (Fig. 1A dashed line). The peak-shape suggests that the mercury adsorption–desorption processes are governed by a Langmuir isotherm in which the interactions between the surface gold atoms and the mercury adatoms play the dominant role.

The addition of sulfate, even at low concentration, to the supporting electrolyte results in significant changes in the voltammetric profile (Fig. 1A, solid line). The most significant was the appearance of two new pairs of sharp peaks (C_1/A_1 and C_2/A_2) superimposed on the previous one and present, respectively, at the initial and final stages of mercury deposition (or dissolution). However, in the region between these two sharp peaks, the voltammetric profile remained essentially unchanged with the wave corresponding to C_m/A_m still clearly visible. This suggests that the addition of sulfate alters the initial and final stages of mercury deposition, with no significant effects during the intermediate stages of deposition.

Changes in the voltammetric profile are more evident when 0.1 M H_2SO_4 is used as supporting electrolyte (Fig. 1B). In this case, the previously mentioned sharp peaks almost completely mask peaks C_m/A_m observed in perchloric acid. Peaks C_1/A_1 move towards negative potentials while C_2/A_2 shift slightly towards positive potentials at this higher (bi)sulfate concentration. Nevertheless, deconvolution of the voltammetric profile between +0.89 and +0.97 V gives rise to three Gaussian peaks that can be associated with those appearing in 0.1 M $HClO_4$ + 1.0 mM H_2SO_4 [26]. This implies that the three processes giving rise to the different pairs of voltammetric peaks for mercury UPD are still present in this electrolyte. Moreover, there is no significant shift in the potential of peaks C_m/A_m, implying that the process is still mainly controlled by the mercury–gold surface interactions. The presence of (bi)sulfate anions in solution appears to be important only at the initial and final stages of the mercury deposition (or desorption) processes, when the sharp peaks C_1/A_1 and C_2/A_2 appear. The processes associated with these peaks are not completely reversible since even at scan rates of 1 mV s^{-1}, the ΔE_p is about 5–10 mV.

Sharp voltammetric peaks, like those found in the presence of (bi)sulfate, are normally associated with phase transitions. In the present case, two phase transitions would ostensibly take place, respectively, at the onset and final stages of mercury deposition/desorption processes. In the case of adsorbed adlayers, phase transitions are generally of the order–disorder type and are associated with the formation/dissolution of ordered structures. In fact, two different structures have been found for Hg UPD over this range of potentials. At potentials above peaks C_1/A_1 a $(\sqrt{3} \times \sqrt{7})$adsorbed (bi)sulfate adlayer has been imaged by STM under very similar experimental conditions [27]. For potentials below peaks C_2/A_2 a $(\sqrt{3} \times \sqrt{19})$ mercurous–sulfate structure has been reported between +0.80 and +0.88 V by GIXD experiments [28].

Generally, order/disorder transitions occur through a nucleation and growth mechanism. In order to determine if this was also the case in the present system, current transients, from potential step chronoamperometric measurements, for the adsorption and desorption processes were obtained. Fig. 2 shows four different desorption transients for the mercury UPD process recorded in 0.1 M H_2SO_4 + 0.10 mM Hg^{2+}. In these experiments, the potential was stepped from an initial value of +0.898 to +0.928 (A), +0.938 (B), +0.942 (C) and +0.946 (D). As can be seen, only the transient in Fig. 2A has an exponential-type decay that can be associated with a process that follows Langmuir desorption kinetics. The other transients exhibited one (Fig. 2B–C) or two (Fig. 2D) shoulders, typical of nucleation processes, superimposed on the exponential decay.

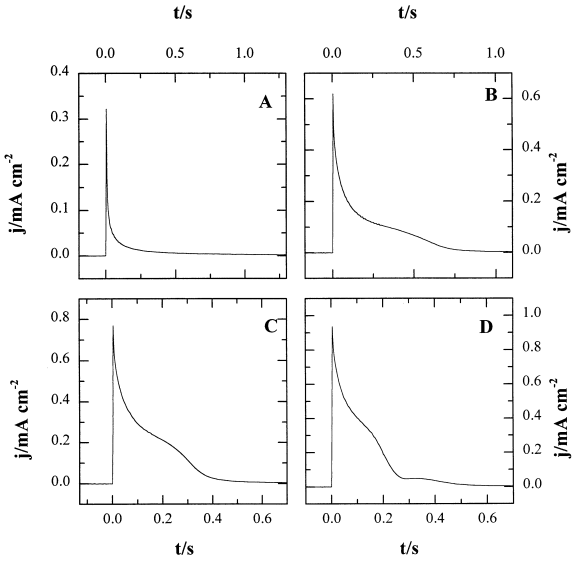

Fig. 2. Current transients for mercury desorption processes on a Au(111) electrode for potential steps from +0.898 V to (A) +0.928 V, (B) +0.938 V, (C) +0.942 V and (D) +0.946 V in 0.10 M H_2SO_4 + 1.0 mM Hg^{2+}.

An analysis of the current transients can provide information on the kinetics of the processes involved. The voltammetric and X-ray measurements have revealed the existence of three different processes consisting of two order/disorder transitions (at the onset and at the end of the desorption process, respectively) and the desorption process itself that follows a Langmuir-type isotherm. The presence of a nucleation and growth mechanism is probably reflected in the shoulders observed in the transients. However, since the order/disorder transitions occur simultaneously with a Langmuir-type desorption process, the shape of the current transients will not necessarily be that expected for a nucleation and growth mechanism alone. According to this model, transients with only one shoulder should be described by an equation con-

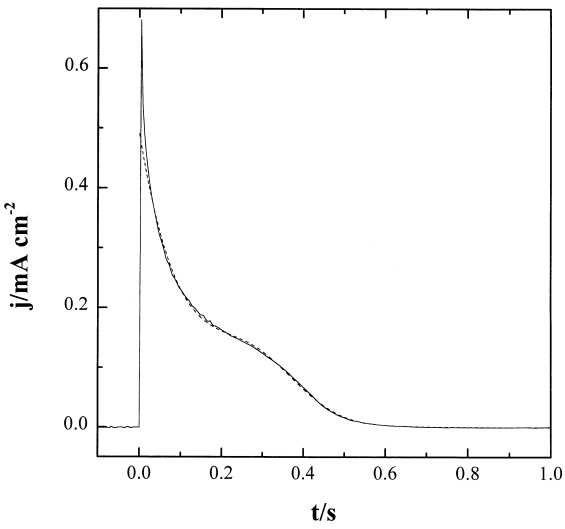

Fig. 3. Current transient for mercury desorption processes on a Au(111) electrode for a potential step from +0.898 to +0.938 V (full line) and fitted curve with a progressive nucleation model (dashed line) in 0.10 M H_2SO_4+1.0 mM Hg^{2+}. See text for details.

taining a Langmuir kinetics term plus a nucleation and growth kinetics term. For the nucleation and growth process the Bewick–Fleischmann–Thirsk (BFT) model was employed in the present case [29,30]. In this approach the equation for the transient is given by:

$$j = k_0 \cdot \exp(-k_1 \cdot t) + j_{max} \cdot \left(\frac{t}{t_{max}}\right)^{n-1} \cdot \times \exp\left[\left(\frac{1-n}{n}\right) \cdot \left(\frac{t}{t_{max}}\right)^{n} - 1\right] \quad (1)$$

where the first term corresponds to the Langmuir kinetics and the second to nucleation and growth. k_0 and k_1 are the parameters for the Langmuir process, j_{max} is the maximum current density for the nucleation and growth process, t_{max} is the time at j_{max} and n is a parameter related to the nucleation mechanism. Generally, an n value of 2 indicates an instantaneous nucleation process whereas an n value of 3 would be indicative of a progressive nucleation process. This equation was used to fit all the experimental results in order to obtain the kinetic parameters.

Fig. 3 shows the transient (full line) for a step from +0.898 to +0.938 V and the fit (dashed line) obtained with Eq. (1) with $n = 3$ (progressive nucleation). As can be observed, the model reproduces quite well the transient measurements. The only (small) deviations occur at short times, when double layer charging processes affect the response. For all the curves with one shoulder, the best fit was obtained for $n = 3$, indicating that the nucleation and growth process proceeds through a progressive nucleation mechanism.

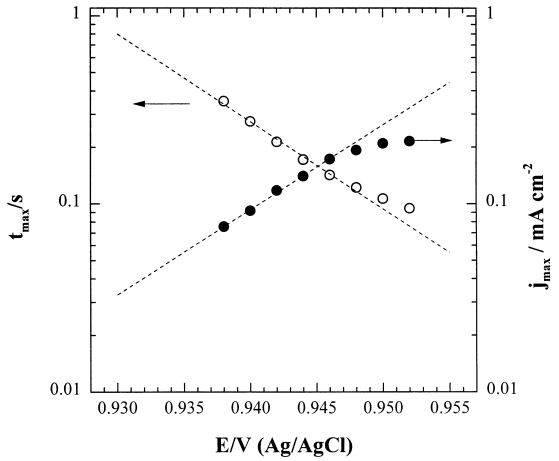

Fig. 4. Plot of t_{max} and j_{max} vs. electrode potential for the current transients for mercury desorption on Au(111) electrodes in 0.10 M H_2SO_4+1.0 mM Hg^{2+}.

Processes following the BFT model should exhibit a linear dependence of $\log(t_{max})$ and $\log(j_{max})$ with potential according to the following relationship [31]:

$$\frac{\partial(\log j_{max})}{\partial E} = -\frac{\partial(\log t_{max})}{\partial E} \quad (2)$$

Fig. 4 shows that both $\log(t_{max})$ and $\log(j_{max})$ are linear with potential for $E < +0.947$ V which correspond, to $t_{max} > 0.13$ s and $j_{max} < 0.13$ mA/cm^2, respectively. As mentioned above, the deviations from linearity at shorter times are likely due to the influence of double layer charging processes. The values of $\partial(\log t_{max})/\partial E$ and $\partial(\log j_{max})/\partial E$ obtained form Fig. 4 are -49 ± 2 and 45 ± 2, respectively, fulfilling, within experimental error, Eq. (2) and thus providing additional evidence of the correctness of the model employed.

No attempt was made to fit the second shoulder that appears at potentials above +0.944 V, since the small charge involved in this feature makes a reliable fit virtually impossible. However, this process is associated with the appearance of peak A_1 in the voltammogram.

An analogous treatment could be carried out for the adsorption (deposition process) although in this case the solution concentration of mercury had to be increased to 10 mM in order to eliminate effects due to diffusion. Fig. 5 shows a deposition transient recorded for a potential step from +0.968 to +0.912 V. This transient is qualitatively very similar to those obtained for the desorption process with a well defined shoulder at about 0.15 s. As for the desorption transients, the best fit to the data (dashed line in Fig. 5) was obtained for a model involving progressive nucleation.

Both mercury adsorption and desorption processes appear to follow a progressive nucleation mechanism.

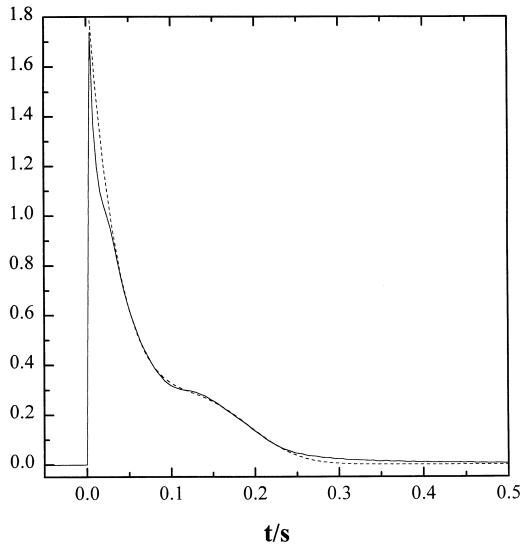

Fig. 5. Current transient for mercury adsorption processes on a Au(111) electrode for a potential step from +0.968 to +0.912 V (full line) and fitted curve with a progressive nucleation model (dashed line) in 0.10 M H_2SO_4 + 10mM Hg^{2+}.

The nucleation process, evident in the transients, appears at potentials that coincide with peaks $C_2\backslash A_2$ in the cyclic voltammogram. We thus conclude that this pair of peaks corresponds to an order–disorder transition associated with the formation of the Hg_2^{2+}-(bi)sulfate ordered adlayer, following a progressive nucleation mechanism. Similarly, we also ascribe peaks $C_1\backslash A_1$ to an order–disorder transition.

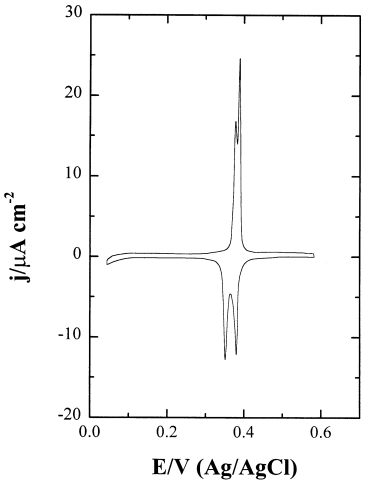

Fig. 6. Voltammetric profile of a Pt(111) electrode in 0.10 M H_2SO_4 + 1.0 mM Cu^{2+}. Scan rate: 1 mV s^{-1}.

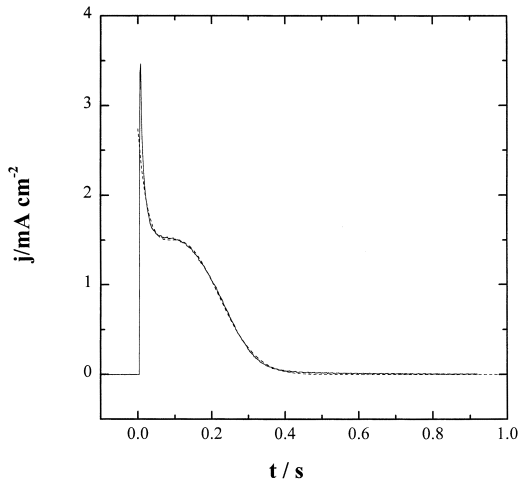

Fig. 7. Current transient for copper desorption processes on a Pt(111) electrode for a potential step from +0.244 to +0.517 V (full line) and fitted curve with a instantaneous nucleation model (dashed line) in 0.10 M H_2SO_4 + 1.0 mM Cu^{2+}.

3.2. Kinetics of Cu UPD on Pt(111) electrodes in the presence of (bi)sulfate anions

The UPD of Cu on Pt(111) electrodes in the presence of bisulfate presents a characteristic voltammetric profile in which the main deposition/stripping peaks appear split (Fig. 6). The splitting depends on the solution concentrations of (bi)sulfate and copper as well as on the scan rate [32]. Different structures have been proposed for this system. At potentials well above the UPD peaks, (bi)sulfate is adsorbed on the electrode surface in a $(\sqrt{3} \times \sqrt{3})R30^\circ$ structure [33]. At potentials closer to the first UPD peak, the adlayer appears to evolve into a $(\frac{2}{1}1_2)$ structure [34, 35]. In the potential region in between both peaks, a honeycomb Cu–(bi)-sulfate structure, similar to that found for the Cu UPD on Au(111) electrodes [36], has been proposed [37]. At potentials below both UPD peaks, a commensurate (1 × 1) Cu structure is formed, on top of which (bi)sulfate is adsorbed with a $(\frac{2}{1}2_1)$ structure [33].

As with the Hg UPD on Au(111) system described previously, the presence of ordered structures can lead to order/disorder transitions on the electrode surface governed by nucleation and growth processes. In order to investigate that possibility, chronoamperometric current/time transients were recorded. Fig. 7 shows a current transient obtained for a potential step from +0.244 to +0.517 V which corresponds to stripping of the commensurate (1 × 1) Cu adlayer. In this case, as with all transients recorded a better fit was always obtained with $n = 2$, that is, the process appears to proceed through an instantaneous nucleation mechanism. As before, j_{max} and t_{max} followed the relationship

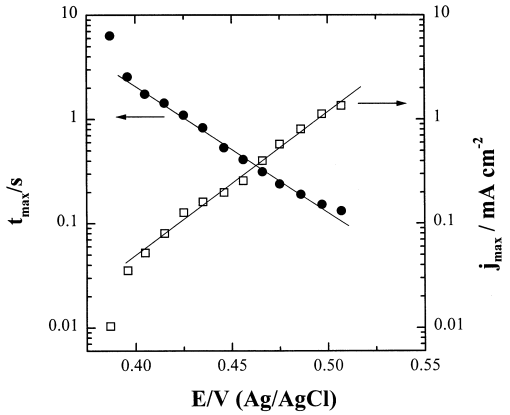

Fig. 8. Plot of t_{max} and j_{max} vs. electrode potential for the current transients for cooper desorption on Pt(111) electrodes in 0.10 M H_2SO_4 + 1.0 mM Cu^{2+}.

predicted by Eq. (2), demonstrating the validity of the model employed (Fig. 8).

There are two main differences with respect to the behavior observed for mercury UPD on Au(111). First, the nucleation mechanism is different. Whereas Hg UPD on Au(111) followed a progressive nucleation mechanism, for Cu UPD on Pt(111), the transients followed an instantaneous nucleation mechanism, meaning that the number of nucleation sites remained constant during the entire transient. The same mechanism has been previously proposed by Kolb et al. for Cu UPD on Au(111) electrodes [20, 21]. In general, two different types of nucleation sites can be found on well-ordered single crystal surfaces: terrace sites and defect sites. Since the number of defect sites on a given surface is constant, a nucleation process controlled by

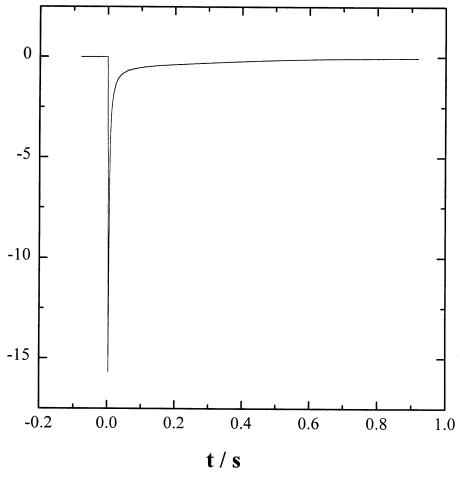

Fig. 9. Current transient for copper adsorption processes on a Pt(111) electrode for a potential step from +0.530 to +0.264 V in 0.10 M H_2SO_4 + 1.0 mM Cu^{2+}.

them should follow an instantaneous nucleation mechanism ($n = 2$). In progressive nucleation, however, there must be a way by which additional nucleation sites are generated at different times. For the Hg UPD on Au(111) electrodes, the proposed mechanism involved the dissolution of the Hg_2^{2+}-(bi)sulfate adlayer with a random desorption following Langmuir kinetics. In this case, some of the vacancies created upon partial dissolution of the adlayer could serve as additional sites for nucleation [38] and thus the increase in the number of nuclei with time.

Along with a different nucleation mechanism, the integrated charge corresponding to the nucleation term in Eq. (1) is quite different in these two cases. The charge ascribed to nucleation in Cu UPD on Pt(111) electrodes represents 75% of the total charge measured during the transient, whereas for the UPD of Hg on Au(111) electrodes it is only 20% of the total charge. This difference can be ascribed to the different nucleation mechanisms. For the Hg UPD, part of the adlayer has to be dissolved via Langmuir kinetics in order to generate additional nuclei. Therefore, the charge for the Langmuir term of the transient is greater relative to the case of an instantaneous nucleation mechanism, where no desorption is required in order to generate nuclei.

The second significant difference is the time scale over which the nucleation process takes place. Comparing t_{max} in Figs. 4 and 8, it can be seen that the Cu UPD on Pt(111) is significantly slower and the nucleation process can be observed over a wider potential range.

For the adsorption process, the transients do not show any evidence of a nucleation process (Fig. 9). In all cases, the transients exhibited a monotonic exponential-type decay. Therefore, for the adsorption step nucleation and growth processes do not appear to be involved.

3.3. Kinetics of the Cu UPD on Pt(111) electrodes in presence of chloride anions

Fig. 10 shows the voltammetric profile of Cu UPD on Pt(111) in 0.1 M $HClO_4$ containing 1 mM of both Cu^{+2} and Cl^-. The profile exhibits two sharp sets of peaks centered at +0.40 and +0.32 V that define three regions where different structures can be found. At potentials above the first UPD peak, chloride anions are adsorbed on the electrode surface in a disordered fashion [38]. As the potential is scanned in the negative direction, copper starts to deposit until an ordered, incommensurate copper–chloride adlayer is formed in the region between both peaks. Using GIXD measurements it has been shown that this adlayer presents a diffraction rod at the (0.765, 0, L) position [39]. After the second UPD peak, a commen-

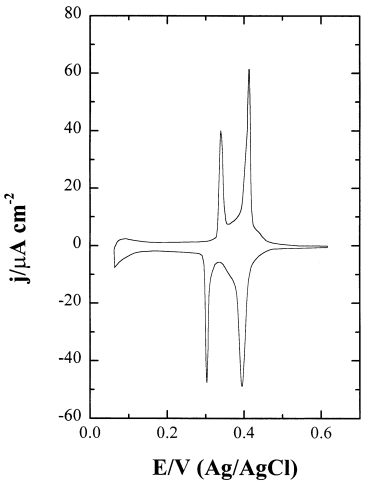

Fig. 10. Voltammetric profile of a Pt(111) electrode in 0.10 M $HClO_4$ + 1.0 mM Cl^- + 1.0 mM Cu^{2+}. Scan rate: 5 mV s^{-1}.

surate (1 × 1) copper adlayer forms on the electrode surface, which, in turn, is covered by a disordered layer of chloride anions [3, 10, 40].

Two different order–disorder transitions occur for this system:

$$\text{Pt–Cl} \leftrightarrow \text{Pt–CuCl (incommensurate)} \quad (3)$$

$$\text{Pt–CuCl (incommensurate)} \leftrightarrow \text{Pt–Cu}(1 \times 1)\text{–Cl} \quad (4)$$

In order to investigate the possible existence or participation of nucleation processes, transients were recorded for potential steps between +0.20 and +0.35 corresponding to the formation of the CuCl bilayer at +0.35 V and its dissolution (and formation of the (1 × 1) copper adlayer) at +0.20 V. Although the transients were not as well-defined as in the presence of bi(sulfate) consistently better fits were obtained for $n = 2$; that is, for an instantaneous nucleation mechanism.

The dynamics of the transition between these ordered layers could also be followed by GIXD measurements. Since the incommensurate CuCl adlayer presents an X-ray diffraction rod at (0.765, 0, 1.5), its scattered intensity could be used to monitor the time evolution of transitions between these two adlayers. To study the dynamics of these structural transitions, the potential step of Fig. 11A was employed. At the initial potential, +0.20 V, the epitaxial copper adlayer is present on the electrode surface. The potential is stepped to +0.35 V at $t = 10$ s, and the incommensurate CuCl structure is formed. The potential is subsequently stepped back to the initial value of +0.20 V at $t = 30$ s. This cycle is repeated in order to obtain appropriate statistics for the simultaneous surface X-ray scattering measurements.

Fig. 11B shows the transient currents obtained for this potential step sequence. As can be seen, the currents (due to the process of Cu deposition/dissolution and the reorganization of the chloride adlayer on the electrode surface) decay to virtually 0 (background) at times well below 1 s following the potential step. However, the X-ray response is completely different (Fig. 11C). In the case of the formation of the incommensurate adlayer, the electrochemical measurements indicate that all the species that constitute the adlayer at this potential are already present on the electrode surface at +0.35 V. In spite of that, the development of the long range periodic order requires significantly longer times then those required for the electrodeposition, implying that the processes of copper and anion adsorption/desorption and the formation of the ordered adlayer occur at different time scales. This situation contrasts with the process leading to the formation of the epitaxial (1 × 1) Cu adlayer from the incommensurate CuCl adlayer. Here, the disappearance of the incommensurate adlayer follows the current response. Therefore, the formation of the incommensurate CuCl adlayer from the epitaxial Cu adlayer has two different and clearly separated steps. First, the desorption of part of the adsorbed Cu and the reorganization of the adsorbed chlorine takes place, giving rise to the electrochemical response.

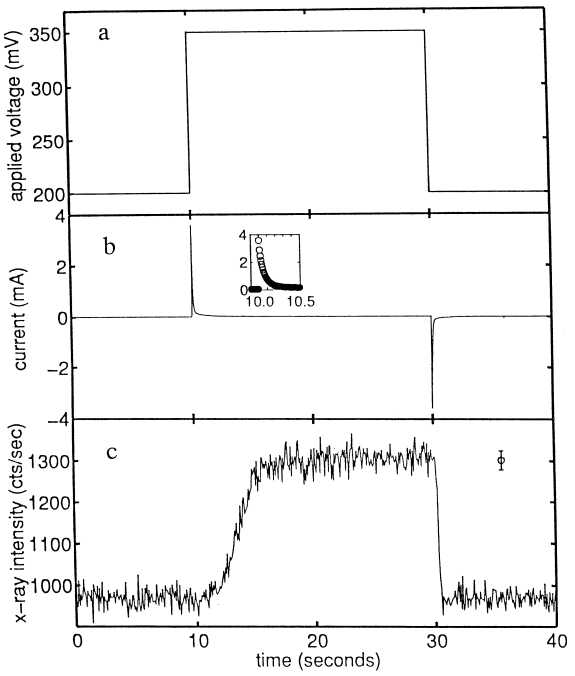

Fig. 11. (a) Applied potential sequence for the X-ray in situ experiments. (b) Current/time response (inset: transient at $t = 10$ s on an extended scale). (c) Time dependence of the scattered X-ray intensity at (0.765, 0, 0.5).

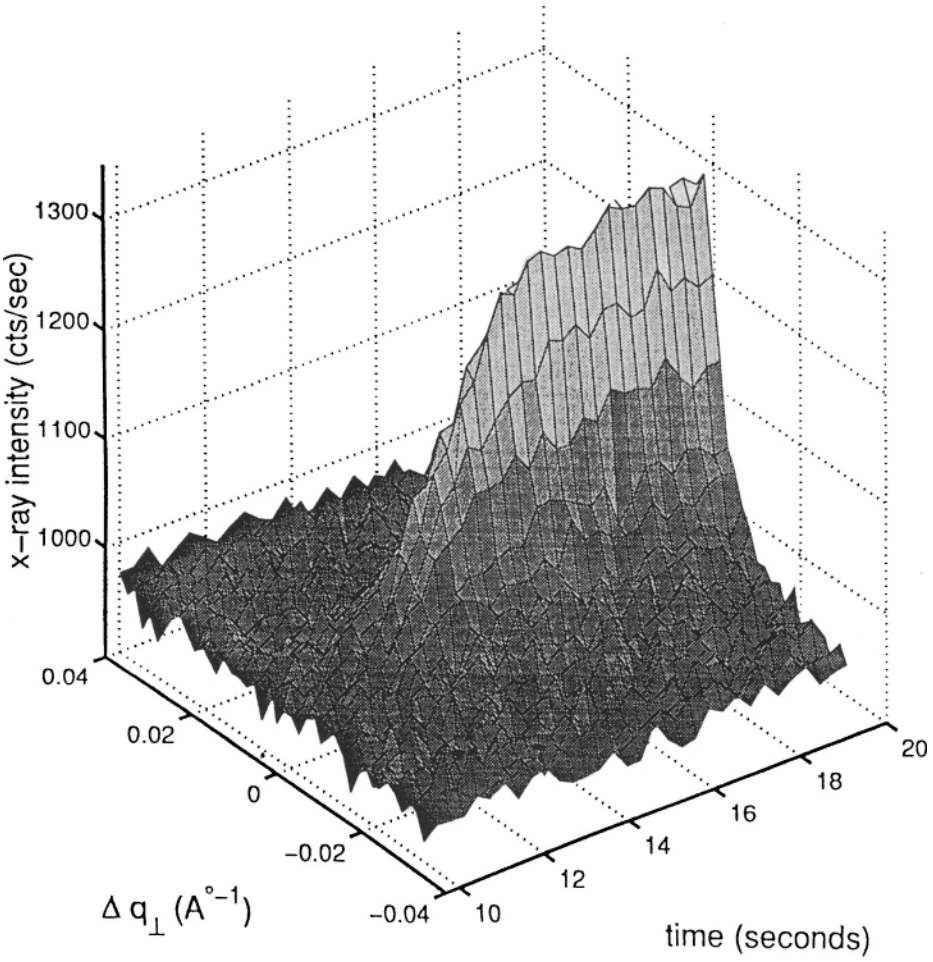

Fig. 12. Plot of scattered intensity as a function of time t, and k at (0.765, k, 1.5).

Subsequently, the formation of the ordered CuCl structure occurs on a much longer time scale.

An alternative that must be considered is the possibility that the diffraction peak could be moving in $q_{\perp}$ or $q_{||}$ as a function of applied potential. At the (0.765, 0, L) position, this would correspond to the overlayer expanding/contracting or rotating with respect to the underlying platinum lattice. Hence, it was necessary to take time-resolved q-scans, rather than simply monitoring the intensity at a single point in reciprocal space. A representative q–t scan is shown in Fig. 12. This scan was taken along the $q_{\perp}$ direction, which has better resolution than $q_{||}$. From these scans and scans along $q_{||}$, it is clear that only the peak intensity varies while its periodicity remains constant in reciprocal space.

By using the three dimensional q–t scans (Fig. 12) it was possible to fit the evolution of the peak and obtain additional information on the island growth. Fitting the peak widths to a Lorentzian line-shape, the inverse of the half-width at half-height of the peak is a length proportional to the diameter of the growing island. Fig. 13 displays a plot of time versus this length. Recall that at time $t = 10$, the potential was stepped from $+0.20$ to $+0.35$ V. Until $t = 12.4$ s, the measured correlation length is effectively zero. Until this point, the island size is either insignificant or too small to measure. After 12.4 s, the islands begin to grow linearly until they reach a saturation point at 200 Å. The island size remains constant at this value until the potential is stepped back to the original value. Thus, this is a measurement of the domain size of the clusters in real-time.

4. Conclusions

These studies illustrate the power of combining electrochemical with in-situ surface X-ray scattering experiments in the understanding of electrodeposition dynamics. This ranges from the mechanisms involved

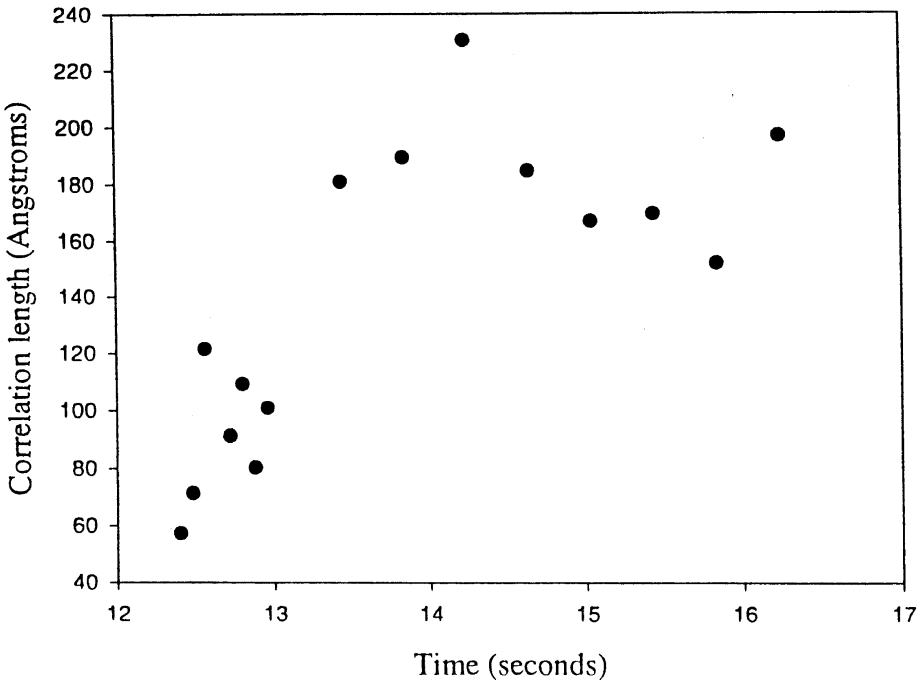

Fig. 13. Correlation length of the growing islands vs. time following a potential step from +0.20 to +0.35 V at time = 10 s.

(e.g. instantaneous vs. progressive nucleation), to the identification of the discrete structures formed and the differences in time-scales that accompany electrochemical events from the achievement of long-range order and island growth.

Acknowledgements

This work was supported by the Office of Naval Research (USA), the National Science Foundation (USA), the Materials Science Center at Cornell University (USA) and the DGES (Spain). EH acknowledges support by a fellowship from the M.E.C. of Spain.

References

[1] D.M. Kolb, in: H. Gerischer, C.W. Tobias (Eds.), Advances in Electrochemistry and Electrochemical Engineering, Vol. 11, Wiley, New York, 1978, p. 125.
[2] R. Adzic, in: H. Gerischer, C.W. Tobias (Eds.), Advances in Electrochemistry and Electrochemical Engineering, Vol. 13, Wiley, New York, 1978, p. 159.
[3] H. Matsumoto, J. Inukai, M. Ito, J. Electroanal. Chem. 379 (1994) 223.
[4] T. Hachiya, H. Honbo, K. Itaya, J. Electroanal. Chem. 315 (1991) 275.
[5] K. Sashikata, N. Furuya, K. Itaya, J. Electroanal. Chem. 316 (1991) 361.
[6] M. Dietterle, T. Will, D.M. Kolb, Surf. Sci. 342 (1995) 29.
[7] C.-H. Chen, S. Vesecky, A.A. Gewirth, J. Am. Chem. Soc. 114 (1992) 451.
[8] C.-H. Chen, K.D. Kepler, A.A. Gewirth, B.M. Ocko, J. Wang, J. Phys. Chem. 97 (1993) 7290.
[9] H.S. Yee, H.D. Abruña, Langmuir 9 (1993) 2460.
[10] R. Gómez, H.S. Yee, G.M. Bommarito, J.M. Feliu, H.D. Abruña, Surf. Sci. 355 (1995) 101.
[11] H.S. Yee, H.D. Abruña, J. Phys. Chem. 97 (1993) 6278.
[12] J.X. Wang, R.R. Adzic, B.M. Ocko, J. Phys. Chem. 98 (1994) 7182.
[13] M.F. Toney, J.G. Gordon, M.G. Samant, G.L. Borges, O.R. Melroy, D. Yee, L.B. Sorensen, J. Phys. Chem. 99 (1995) 4733.
[14] A. Bewick, B. Thomas, J. Electroanal. Chem. 84 (1977) 127.
[15] J.W. Schultze, D. Dickerman, Ber. Bunsenges. Phys. Chem. 82 (1978) 528.
[16] J.W. Schultze, D. Dickerman, Faraday Symp. Chem. Soc. 37 (1977) 36.
[17] G. Staikov, K. Jüttner, W.J. Lorenz, E. Schmidt, Electrochim. Acta 23 (1978) 305.
[18] J.N. Jovicevic, V.D. Jovic, A.R. Despic, Electrochim. Acta 29 (1984) 1625.
[19] V.D. Jovic, J.N. Jovicevic, A.R. Despic, Electrochim. Acta 30 (1985) 1455.
[20] M.H. Hölze, U. Retter, D.M. Kolb, J. Electroanal. Chem. 371 (1994) 101.
[21] M.H. Hölze, U. Retter, D.M. Kolb, Electrochim. Acta 40 (1995) 1237.

[22] J. Clavilier, D. Armand, S.G. Sun, M. Petit, J. Electroanal. Chem. 205 (1986) 267.
[23] M.G. Samant, M.F. Toney, G.L. Borges, L. Blum, O.R. Melroy, Surf. Sci. Lett. 193 (1988) L29.
[24] B.M. Ocko, J. Wang, A. Davenport, H. Isaacs, Phys. Rev. Lett. 65 (1990) 1466.
[25] J. Wang, B.M. Ocko, A.J. Davenport, H.S. Isaacs, Phys. Rev. B 46 (1992) 10321.
[26] E. Herrero, H.D. Abruña, Langmuir 13 (1997) 4446.
[27] J. Inukai, S. Sugita, K. Itaya, J. Electroanal. Chem. 403 (1996) 159.
[28] J. Li, H.D. Abruña, J. Phys. Chem. B 101 (1997) 2907.
[29] A. Bewick, M. Fleischmann, H.R. Thirsk, Trans. Faraday. Soc. 58 (1962) 2200.
[30] M. Fleischmann, H.R. Thirsk, in: P. Delehay (Ed.), Advances in Electrochemistry and Electrochemical Engineering, Vol. 3, Wiley, New York, 1963, p. 123.
[31] D.D. Macdonald, Transient Techniques in Electrochemistry, Plenum, New York, 1977, p. 277.
[32] N.M. Markovic, P.N. Ross, Langmuir 9 (1993) 580.
[33] K. Sashikata, N. Furuya, K. Itaya, J. Electroanal. Chem. 316 (1991) 361.
[34] A.M. Funtikov, U. Linke, U. Stimming, R. Vogel, Suf. Sci. 324 (1995) L343.
[35] A.M. Funtikov, U. Stimming, R. Vogel, J. Electroanal. Chem. 428 (1997) 147.
[36] M.F. Toney, J.N. Howard, J. Richer, G.L. Borges, J.G. Gordon, O.R. Melroy, Phys. Rev. Lett. 75 (1995) 4772.
[37] C.A. Lucas, N.M. Markovic, P.N. Ross, Phys. Rev. B 56 (1997) 3651.
[38] B.N. Ocko, G.M. Watson, J. Wang, J. Phys. Chem. 98 (1994) 897.
[39] I.M. Tidswell, C.A. Lucas, N.M. Markovic, P.N. Ross, Phys. Rev. B 51 (1995) 10205.
[40] D.M. Kolb, A. Jaaf-Golze, M.S. Zei, Dechema Monographien, Vol. 102, VCH, Germany, 1986, p. 53–64.